CURRENT PREDICTION CONTROL FOR SWITCHED RELUCTANCE MOTORS IN AGRICULTURAL MACHINERY FITTING

Yuanyuan LI[1,*], Suling TIAN[1], Yushuang ZHANG[1]

Switched Reluctance Motors (SRMs) are widely used in agricultural machinery due to their simple construction and high reliability. However, the current regulation of high-power SRMs has been a persistent challenge due to their low phase inductance and limited current sampling rates. This paper proposes a fixed-frequency current prediction control method to address this issue. The method discretizes the voltage equation to predict the root mean square (RMS) voltage required for the next modulation step. Additionally, to obtain the incremental inductance parameters required for the current prediction algorithm, a combination of chopping-mode rotational measurement and Fourier series fitting is employed to accurately extract incremental inductance data across all rotor positions of the SRM. Furthermore, to address the one-step delay problem inherent in digital implementations, a delay compensation strategy is introduced to reduce the current ripple caused by this delay. Simulation and experimental results on a low-inductance 6/4 SRM demonstrate the effectiveness of the proposed algorithm in improving current tracking performance and reducing ripple.

Keywords: Switched Reluctance Motors, Current prediction, Incremental inductance, One-step delay

1. Introduction

In industrial and commercial applications that demand high cost-effectiveness, fault tolerance, and reliability—such as mining vehicle motor drive systems and aerospace starter-generator systems—motor performance is essential. Traditionally, induction motors (IMs) and permanent magnet synchronous motors (PMSMs) have dominated these areas. However, their structural designs and drive topologies impose inherent limitations, making them increasingly inadequate for meeting the stricter performance requirements of modern applications [1]. For example, PMSMs rely on rare earth materials, resulting in higher costs and supply chain risks, while IMs tend to have lower efficiency and require more maintenance [2-5].

In contrast, switched reluctance motors (SRMs) offer several advantages that make them well-suited for diverse applications, including agricultural machinery [6-7]. The robust construction of SRMs, featuring a simple rotor and stator design with no permanent magnets or windings on the rotor, ensures high

[1] School of Mechanical and Electrical Engineering, East University of Heilongjiang, Harbin, China
* Corresponding author, e-mail: liyuanyuan1@hljeu.edu.cn

reliability and durability in harsh operating environments such as those encountered in agricultural fields. Additionally, the fault-tolerant drive topology of SRMs makes them an ideal choice for agricultural equipment that demands uninterrupted operation under varying load conditions. Their ability to operate efficiently over a wide speed range also aligns well with the diverse mechanical requirements of agricultural machinery, such as tractors, harvesters, and irrigation pumps. Moreover, the low manufacturing cost of SRMs, coupled with their capability to handle frequent starts, stops, and load variations, further enhances their appeal for cost-sensitive and performance-critical applications in agriculture.

Despite their advantages, SRMs are not without challenges. Key issues such as torque ripple, which arises from the nonlinear relationship between electromagnetic torque and current, and mechanical noise caused by rotor radial distortions, significantly hinder their deployment in high-performance domains. These problems reduce the appeal of SRMs for applications requiring precise control, smooth operation, and low acoustic emissions. Addressing these challenges necessitates focused efforts in both motor design and control algorithm development [7].

The goal of motor design improvements is to optimize the static torque-position characteristics of SRMs. This can be achieved by implementing reasonable slot-pitch combinations, altering the stator and rotor pole pitch, and modifying pole shapes. These measures aim to reduce torque ripple while maintaining the same current conditions [8]. However, while such design modifications are effective, they often introduce trade-offs. For example, increasing the number of phases or poles improves performance but requires additional switching devices, thereby complicating the design and reducing manufacturing efficiency. Similarly, employing uneven airgap designs can minimize torque ripple but restricts the motor to unidirectional operation.

In comparison, addressing torque ripple through control algorithms is more universally applicable and adaptable to varying operating conditions. With the widespread adoption of digital control chips, the implementation and migration of control algorithms have become increasingly convenient. Advanced low-torque-ripple control strategies have emerged as a research focus in SRM systems [9].

By employing torque control concepts, reference current waveforms corresponding to smooth torque can be derived. These waveforms enable closed-loop current control to suppress torque ripple effectively [10]. In this approach, the precision and ripple of current control are critical factors directly affecting the overall control performance. For low-speed SRMs, hysteresis controllers can be utilized for phase current control due to their relatively large design inductance. However, for high-speed and high-power SRMs, current control becomes significantly more challenging [11].

At high speeds, the rapid rise and fall times of the reference current severely

constrain control performance. To address this, high-speed SRMs are typically designed with low-turns, low-inductance winding structures that facilitate rapid current changes. However, these designs result in higher back electromotive force (EMF) at rated speeds, necessitating a control system with a higher bus voltage. Under such conditions, the voltage across the windings can equal the bus voltage, leading to a large di/dt and substantial current ripple when the control frequency is insufficient. Such ripple can damage switching devices and motor components, as demonstrated in [12], where a 45kW high-speed SRM operating at 20 kHz with a 600 A current exhibited a ripple of 200 A, causing the hysteresis controller to fail.

To mitigate current ripple, various novel control strategies have been proposed [11]. These include improved hysteresis control, PWM, and sliding mode control. While improved hysteresis control can partially reduce di/dt, it is ineffective for high rates of current change. Sliding mode control combined with PWM can theoretically minimize current fluctuations but requires high current sampling and control frequencies, often necessitating analog circuits, which are unsuitable for modern digital control systems. PI controllers combined with PWM offer another approach by leveraging the insensitivity of PI controllers to model variations. However, PI controllers suffer from phase lag in their control output, and a single set of PI parameters is insufficient to address varying operating conditions effectively.

Predictive control has emerged as a novel control algorithm in recent years [13], demonstrating excellent dynamic response and gaining widespread industrial application [14]. This method offers a promising solution for mitigating current ripple in SRMs.

In this paper, a fixed-frequency current prediction control strategy for switched reluctance motors (SRMs) is proposed. By discretizing the voltage equation and utilizing real-time motor state feedback, the optimal RMS voltage for the next step is predicted to achieve precise current tracking. To address the issue of model dependency commonly encountered in predictive control, a Fourier-based curve-fitting approach is employed. This method effectively stores incremental inductance data with high fidelity in a compact format, enabling efficient deployment in embedded control systems.

Distinct from previous studies, the proposed approach features three key innovations: (1) a practical method for fitting SRM incremental inductance using Fourier series based on data measured under actual rotating conditions, offering a lightweight and accurate alternative to finite element modeling or neural network approximations; (2) an explicit compensation mechanism for computational delay, which enhances real-time control accuracy; and (3) a simplified predictive control structure that balances performance and computational efficiency, making it well-suited for low-cost microcontroller platforms. In addition, the proposed method emphasizes low-speed current control performance, a condition often overlooked

yet critical in many practical SRM applications.

To validate the effectiveness of the proposed strategy, both simulations and experimental tests are conducted. The results demonstrate significant improvements in current ripple suppression and overall system stability.

2. SRM Control Theory Based on Current Prediction Control

2.1 Continuous Mathematical Model and Analysis of SRM

Due to the doubly salient structure and concentrated windings of SRM, its core losses and inter-phase mutual inductance can be neglected during analysis [15]. At this point, the phase voltage equation of the SRM can be expressed as:

$$\begin{aligned} U(t) &= Ri(t) + \frac{d\psi(\theta,i)}{dt} \\ &= Ri(t) + \frac{\partial\psi(\theta,i)}{\partial i}\frac{di}{dt} + \frac{\partial\psi(\theta,i)}{\partial\theta}\frac{d\theta}{dt} \\ &= Ri(t) + \frac{\partial\psi(\theta,i)}{\partial i}\frac{di}{dt} + \frac{\partial\psi(\theta,i)}{\partial\theta}\omega \end{aligned} \tag{1}$$

Where R represents the equivalent phase resistance of the SRM; ψ denotes the phase flux linkage, which is a nonlinear function of the rotor angle θ and the phase current i; and ω is the rotor angular velocity.

Equation (1) indicates that the balanced phase voltage of the SRM consists of three components. The first component is the voltage drop across the equivalent resistance; the second component is the induced (EMF caused by the variation of flux linkage with current; and the third component is the motional EMF resulting from the change in flux linkage with respect to the rotor angle. It is evident that traditional control methods, such as current chopping control, angle position control, and PI combined with PWM, do not quantitatively utilize the voltage equation, leading to inaccuracies in current tracking and consequently resulting in significant current ripple.

2.2 Principle of SRM Current Prediction Control

Under the condition of a sufficiently high modulation frequency, Equation (1) can be discretized using the Forward Euler method as:

$$\begin{aligned} U(k+1) &= i_{\text{ref}}(k+1)R \\ &+ \frac{\psi(i_{\text{ref}}(k+1),\theta(k)) - \psi(i(k),\theta(k))}{i_{\text{ref}}(k+1) - i(k)}\frac{i_{\text{ref}}(k+1) - i(k)}{T} \\ &+ \frac{\psi(i_{\text{ref}}(k+1),\theta_{\text{est}}(k+1)) - \psi(i_{\text{ref}}(k+1),\theta(k))}{\theta_{\text{est}}(k+1) - \theta(k)}\frac{\theta_{\text{est}}(k+1) - \theta(k)}{T} \end{aligned} \tag{2}$$

Where $U(k+1)$ represents the effective voltage at time step $(k+1)$, and $i_{\text{ref}}(k+1)$ denotes the current at time step $(k+1)$.

According to the principle of predictive control, i_{ref}(k+1) is defined as the current reference at time step (k+1), while $\theta(k+1)$ denotes the rotor position at time step (k+1), and T represents the PWM period. It is worth noting that, to achieve significant control effects and conclusions, this paper adopts a flat-topped pulse waveform for i_{ref}(k+1), consistent with the chopping waveform. For practical applications requiring smooth torque, i_{ref}(k+1) should instead correspond to a reference current profile designed to produce smooth torque.

Further analysis of the discretized voltage equation reveals that the discretized induced EMF is:

$$\begin{aligned} e_{in}(k+1) &= \frac{\psi(i_{\text{ref}}(k+1),\theta(k)) - \psi(i(k),\theta(k))}{i_{\text{ref}}(k+1) - i(k)} \frac{i_{\text{ref}}(k+1) - i(k)}{T} \\ &= L_{\text{inc}}(i(k),\theta(k)) \frac{i_{\text{ref}}(k+1) - i(k)}{T} \end{aligned} \tag{3}$$

In the equation, $L_{\text{inc}}(i(k), \theta(k))$ represents the incremental inductance at time k, which is a pre-measured parameter.

The discretized motional EMF is:

$$e_{sp}(k) = \frac{\psi(i_{\text{ref}}(k+1),\theta_{\text{est}}(k+1)) - \psi(i_{\text{ref}}(k+1),\theta(k))}{\theta_{\text{est}}(k+1) - \theta(k)} \omega(k+1) \tag{4}$$

Where $\omega(k+1)$ represents the rotor angular velocity at time step (k+1).

Given the sufficiently high control frequency and the effect of rotational inertia, the rate of change of current is significantly faster than that of the rotor speed. As a result, it can be reasonably concluded that:

$$\begin{cases} \omega(k+1) \approx \omega(k) \\ e_{sp}(k+1) \approx e_{sp}(k) \end{cases} \tag{5}$$

It is assumed that the back EMF at the next time step remains unchanged from the current time step. Accordingly, the motional EMF at the current step can be expressed based on the calculation result obtained in the previous step:

$$e_{sp}(k) = u(k) - i(k)R - L_{\text{inc}}(i(k-1),\theta(k-1)) \frac{i(k) - i(k-1)}{T} \tag{6}$$

At this point, all parameters on the right-hand side of Equation (2) are known, allowing the complete calculation of the effective voltage for the next cycle and subsequent modulation.

3. Acquisition of Incremental Inductance and One-Step Delay Compensation

3.1 Principle of SRM Current Prediction Control

In Equation (3), the SRM incremental inductance parameters are required. Therefore, it is necessary to fit and store these inductance values as prior parameters.

This paper uses a chopping current control method to measure the actual incremental inductance information while the SRM is in a rotating state. A Fourier-based fitting approach is then used to fit the incremental inductance curve for all positions, thereby improving control accuracy.

The current waveform of the chopping control method is shown in Fig. 1, where $i_{\max}$ and $i_{\min}$ are the upper and lower limits of the chopping range.

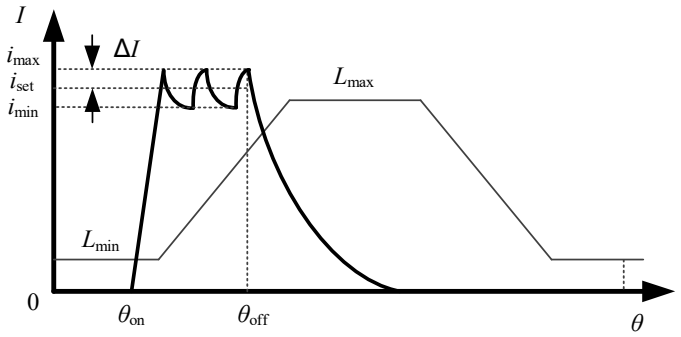

Fig. 1. Schematic Diagram of the Chopping Measurement Method

During the rise and fall intervals of the current in the chopping process, the voltage equations are expressed as follows:

$$\begin{aligned} U_{\mathrm{dc}} &= 2U_{\mathrm{dio}} + Ri_{+} + \frac{\partial \psi}{\partial i_{+}}\frac{di_{+}}{dt} + \frac{\partial \psi}{\partial \theta}\frac{d\theta}{dt} \\ &= 2U_{\mathrm{dio}} + Ri_{+} + L_{\mathrm{inc}}(\theta, i)\frac{di_{+}}{dt} + i\frac{\partial L_m}{\partial \theta}\omega \end{aligned} \tag{7}$$

$$\begin{aligned} -U_{\mathrm{dc}} &= 2U_{\mathrm{dio}} + Ri_{-} + \frac{\partial \psi}{\partial i_{-}}\frac{di_{-}}{dt} + \frac{\partial \psi}{\partial \theta}\frac{d\theta}{dt} \\ &= 2U_{dio} + Ri_{-} + L_{\mathrm{inc}}(\theta, i)\frac{di_{-}}{dt} + i\frac{\partial L_m}{\partial \theta}\omega \end{aligned} \tag{8}$$

When the chopping control frequency is relatively high, the hysteresis band becomes sufficiently narrow, and $i_{\max}$ and $i_{\min}$ can be approximated as equal. Thus, Equations (7) and (8) are simplified as:

$$2U_{\mathrm{dc}} = L_{\mathrm{inc}}(\theta, i)\left(\frac{di_{+}}{dt} + \frac{di_{-}}{dt}\right) \tag{9}$$

From Equation (9), it can be observed that the chopping-based method for measuring incremental inductance effectively eliminates measurement errors caused by diode voltage drops and voltage drops across equivalent resistance. Additionally, it avoids inaccuracies resulting from inter-phase magnetic coupling effects that commonly occur during static measurements. The raw incremental inductance data obtained using this method are presented in Fig. 2.

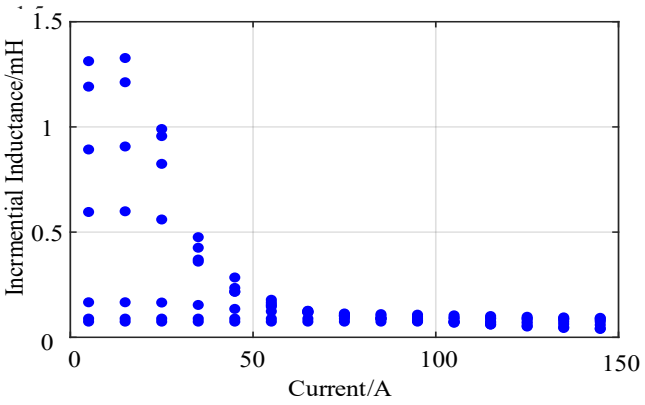

Fig. 2. Raw Data of Incremental Inductance

Considering that the incremental inductance curve exhibits sinusoidal characteristics and is symmetric about 45 degrees, it can be decomposed into a Fourier series and fitted as a combination of the fundamental component and its harmonics. For a function $f(t)$ with a period T, the fundamental frequency is $\omega=2\pi/T$. When the Dirichlet conditions are satisfied, it can be expanded into a Fourier series. Taking the SRM incremental inductance $L_{inc}(i, \theta)$ as an example, its period is $T=2\pi/N_r$ where Nr is the number of rotor poles, and it can be expanded into a Fourier series:

$$L_{inc}(\theta,i) = L_{inc0}(i) + \sum_{n=1}^{\infty}[L_{inc1n}(i)\cos(nN_r\theta) + L_{inc2n}(i)\sin(nN_r\theta)] \quad (10)$$

Since $L_{inc}(\theta, i)$ is symmetric about the Y-axis, the DC component is 0. Therefore:

$$L_{inc}(\theta,i) = L_{inc0}(i) + \sum_{n=1}^{\infty}[L_{inc1n}(i)\cos(nN_r\theta)] \quad (11)$$

Considering the computational cost, the order of the fitting formula should be reasonably selected. Repeated calculations and experiments show that using up to the 6th harmonic achieves a high fitting accuracy. At this point, Equation (11) can be further simplified as:

$$\begin{aligned} L_{inc}(\theta,i) = {} & L_{inc0}(i) + L_{inc1}(i)\cos(4\theta) + L_{inc2}(i)\cos(8\theta) \\ & + L_{inc3}(i)\cos(12\theta) + L_{inc4}(i)\cos(16\theta) \\ & + L_{inc5}(i)\cos(20\theta) + L_{inc6}(i)\cos(24\theta) \end{aligned} \quad (12)$$

In Equation (10), there are 7 coefficients: $L_{inc0}(i)$ $L_{inc1}(i)$ $L_{inc2}(i)$, $L_{inc3}(i)$, $L_{inc4}(i)$, $L_{inc5}(i)$ and $L_{inc6}(i)$ When the current is fixed, 7 specific positions need to be selected to obtain 7 specific incremental inductance values to determine the coefficients. To ensure even distribution, the specific positions are chosen as

θ_0=0°θ_1=7.5°, θ_2=12°, θ_3=22.5°, θ_4=30°, θ_5=37.5°, θ_6=45°

Substituting these into Equation (12) gives:

$$\begin{bmatrix} L_{inca}(i) \\ L_{incb}(i) \\ L_{incc}(i) \\ L_{incd}(i) \\ L_{ince}(i) \\ L_{incf}(i) \\ L_{incg}(i) \end{bmatrix} = T^s \begin{bmatrix} L_{inc0}(i) \\ L_{inc1}(i) \\ L_{inc2}(i) \\ L_{inc3}(i) \\ L_{inc4}(i) \\ L_{inc5}(i) \\ L_{inc6}(i) \end{bmatrix} \tag{13}$$

Where T^s is a matrix, specifically expressed as:

$$\begin{bmatrix} 1\cos(4\theta_0) & \cos(8\theta_0) & \cos(12\theta_0) & \cos(16\theta_0) \\ 1\cos(4\theta_1) & \cos(8\theta_1) & \cos(12\theta_1) & \cos(16\theta_1) \\ 1\cos(4\theta_2) & \cos(8\theta_2) & \cos(12\theta_2) & \cos(16\theta_2) \\ 1\cos(4\theta_3) & \cos(8\theta_3) & \cos(12\theta_3) & \cos(16\theta_3) \\ 1\cos(4\theta_4) & \cos(8\theta_4) & \cos(12\theta_4) & \cos(16\theta_4) \\ 1\cos(4\theta_5) & \cos(8\theta_5) & \cos(12\theta_5) & \cos(16\theta_5) \\ 1\cos(4\theta_6) & \cos(8\theta_6) & \cos(12\theta_6) & \cos(16\theta_6) \end{bmatrix} \tag{14}$$

The inverse of T^s can be used to obtain the fitting matrix. By combining the original incremental inductance data with the Fourier fitting method, the incremental inductance parameters of the SRM for all rotor positions can be obtained, as shown in Fig. 3. When the current is relatively small, the incremental inductance changes linearly with the current; as the current increases, the incremental inductance rapidly decreases and approaches saturation, which is consistent with the characteristics of the SRM. This qualitatively confirms that the measurement and fitting methods are fundamentally correct.

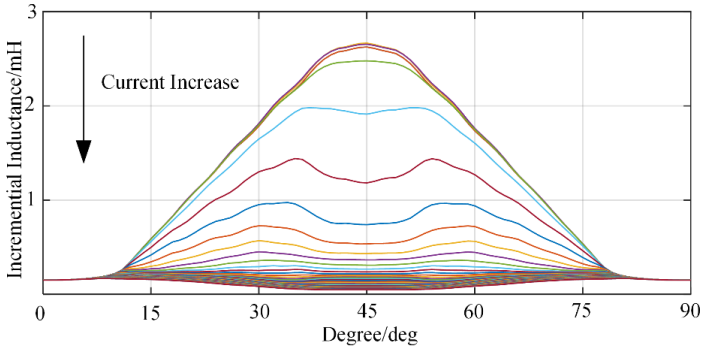

Fig. 3. Incremental Inductance Parameters of SRM Across All Rotor Positions

Notably, by using the incremental inductance fitting function, it is only necessary to store the inductance values at seven specific rotor positions. Through Fourier series reconstruction, the complete incremental inductance profile over the full angular range can be accurately derived, thereby significantly reducing storage requirements.

In numerical control systems, delays can be caused by various factors, including current sampling latency, controller computation time, and switching signal transition delays. Among these, the current sampling delay accounts for the largest proportion, primarily resulting in a one-step delay in the controller's duty cycle output. Specifically, the voltage calculated at the current time step should ideally be applied within the same cycle, but due to the sampling delay, this voltage only affects the switching devices in the next cycle. Fig. 4 illustrates the cause of the one-step delay.

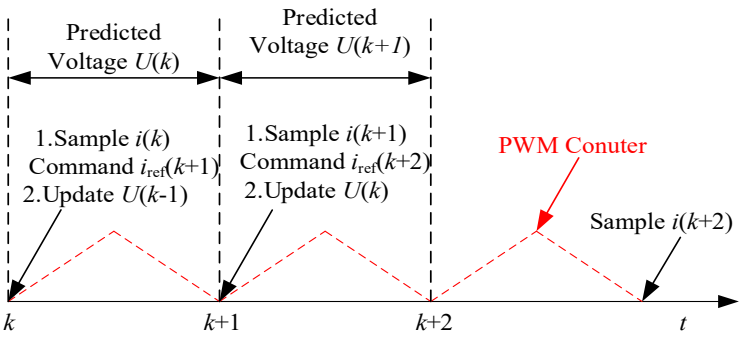

Fig. 4. Incremental Inductance Parameters of SRM Across All Rotor Positions

For SRMs, due to their small inductance and independent modulation of each phase, only one effective voltage value can be output within each modulation cycle. Modulating the calculated voltage with a one-step delay results in significant errors, causing current tracking errors.

By ignoring minor delay factors and considering only the primary delay

caused by current sampling, the reference current can be delayed by one step. Iterative computation can then be performed using the known parameters and unknown parameters over three steps. In this case, let:

$$i_{\text{ref}}(k+2)=i^{*}(k+1) \tag{15}$$

The purpose of Equation (15) is to proactively delay the predicted voltage by one step, i.e., to calculate the voltage two steps in advance. It is important to note that when calculating the voltage for the second step, $i(k+1)$ is derived from Equation (2). Therefore, the essence of the one-step compensation is to use the voltage equations and related parameters from two steps in an iterative manner within one control cycle, thereby compensating for sampling delay errors. The compensated voltage equation is as follows:

$$U(k+2)=i_{\text{ref}}(k+2)R+L_{\text{inc}}(k+1)\frac{i_{\text{ref}}(k+2)-i(k+1)}{T}+e(k) \tag{16}$$

As analyzed earlier, the reference current is delayed by one step before being input into the current inner loop. Simultaneously, the measured SRM current and rotor speed are sent to the controller to compute $U(k+2)$. The control system block diagram is shown in Fig. 5.

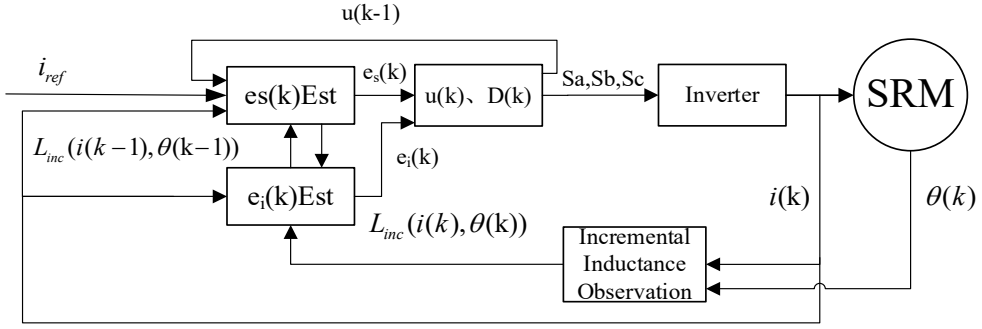

Fig. 5. Block Diagram of Current Prediction Inner Loop Control

4. Simulation Verification

To verify the effectiveness of the proposed current prediction control strategy, a comprehensive simulation model was developed using Simulink. The model incorporates a 6/4 SRM powered by a 150V DC source, with the current prediction algorithm operating at a switching frequency of 10 kHz. This simulation environment was carefully designed to mimic real-world operational conditions and ensure that the proposed control strategy could be rigorously evaluated.

For comparison, a conventional chopping control strategy was also implemented in the simulation. To protect the system from excessive current, a limiter module was introduced to cap the current at the maximum allowable value, ensuring safe operation throughout the process. The simulations were conducted

under different operational conditions, including rotational speeds of 800 rpm and 1500 rpm, to evaluate the algorithm's performance across a range of scenarios. A reference tracking current of 150A was applied to test the system's ability to maintain accurate current tracking.

The specific parameters of the motor used in the simulation are detailed in Table 1, providing a clear basis for reproducibility and comparison. The steady-state results for the A-phase current reference and the actual current output are presented in Fig. 6 and Fig. 7, illustrating the system's behavior under the given conditions. These results demonstrate that the proposed control strategy can achieve precise current tracking, thereby enhancing the overall performance and stability of SRM systems. A detailed analysis of the simulation results confirms the effectiveness of the proposed current prediction algorithm, providing a solid foundation for subsequent experimental validation and practical implementation.

Table 1

Parameters of the Simulated SRM

Motor Parameter	Value
Stator Resistance	0.02 Ω
Inertia	0.0005 kg·m²
Friction Coefficient	0.003 N·m·s
Unaligned Inductance	0.5 mH
Aligned Inductance	1 mH
Saturated Aligned Inductance	0.15 mH
Maximum Current	250 A

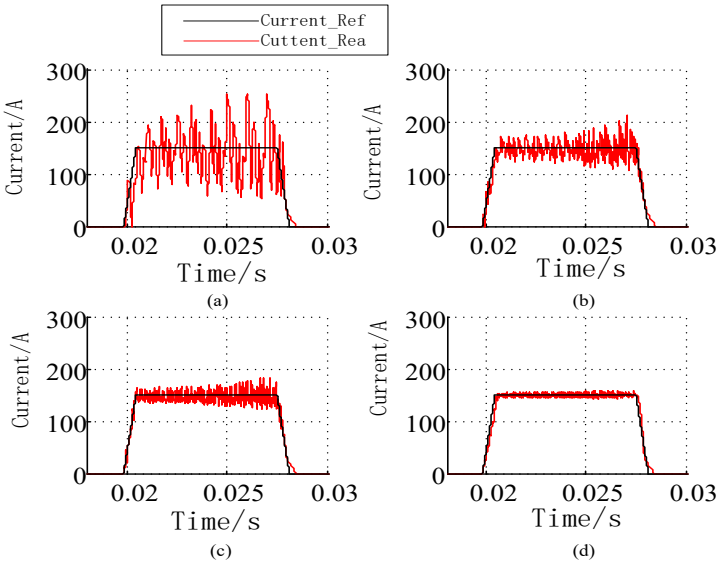

(a) Chopping at 10 kHz; (b) Chopping at 40 kHz; (c) Chopping at 80 kHz; (d) Current Prediction at 10 kHz

Fig. 6. Simulated Current Waveforms at 800 rpm

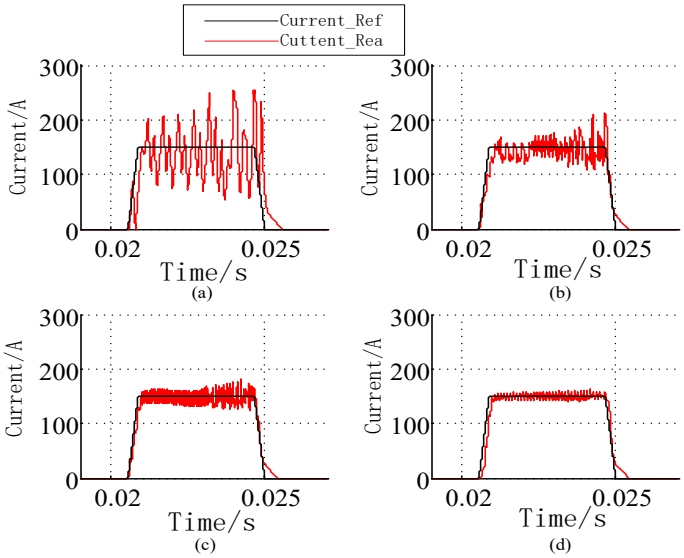

(a) Chopping at 10 kHz; (b) Chopping at 40 kHz; (c) Chopping at 80 kHz; (d) Current Prediction at 10 kHz

Fig. 7. Simulated Current Waveforms at 1500 rpm

5. Experimental Validation

To assess the effectiveness of the proposed current prediction algorithm, an experimental test platform was built using the TMS320F28335 digital signal processor, as illustrated in Fig. 8. The experimental setup employed the same motor parameters as those used in the simulation for consistency and comparability. To safeguard the power module and the motor, a chopping algorithm operating at a control frequency of 40 kHz was also implemented for comparison against the proposed predictive control strategy.

The detailed hardware configuration of the experimental platform is summarized in Table.2.

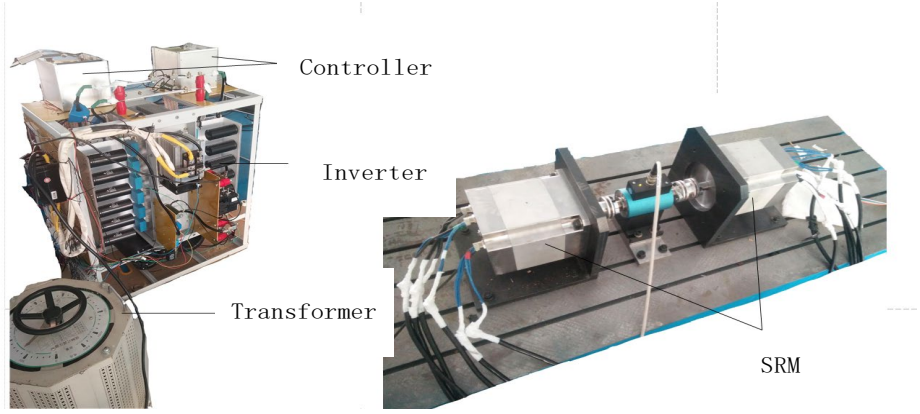

Fig. 8. Experimental Platform

Table 2

Parameters of the experiment platform

Motor Parameter	Value Same as simulation model
DC Bus Voltage	150 V
Power Switch	Infineon FF300R12ME4 IGBT
Current Sensor	LA 205
DC Bus Capacitance	6 × 2200 μF electrolytic capacitors
Controller	TI DSP28335 + ADI AD7606 ADC

The experimental results, shown in Fig. 9 and Fig. 10, reveal a high degree of consistency with the simulation outcomes.

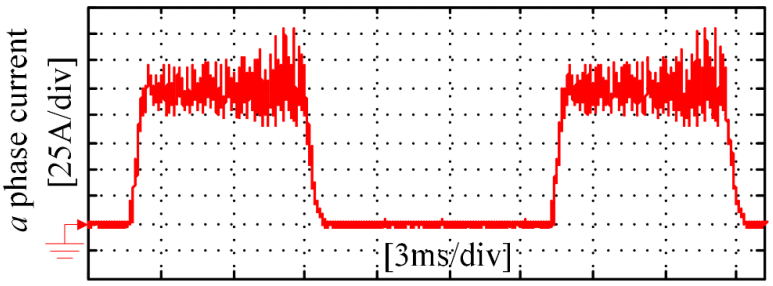

(a) Chopping at 40 kHz

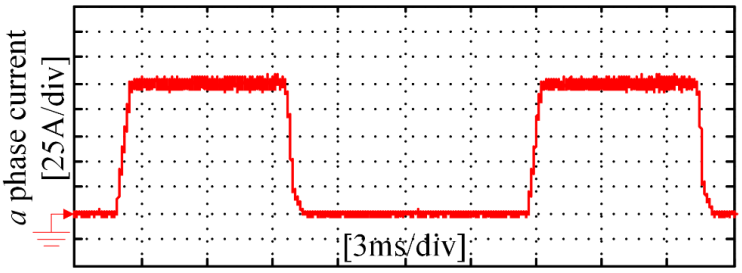

(b) Current Prediction at 10 kHz

Fig. 9. Experimental Current Waveforms at 800 rpm

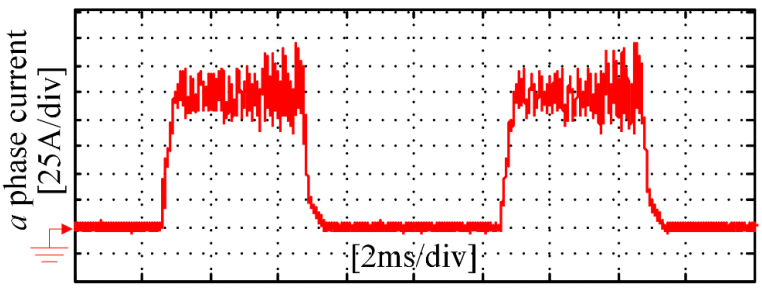

(a) Chopping at 40 kHz

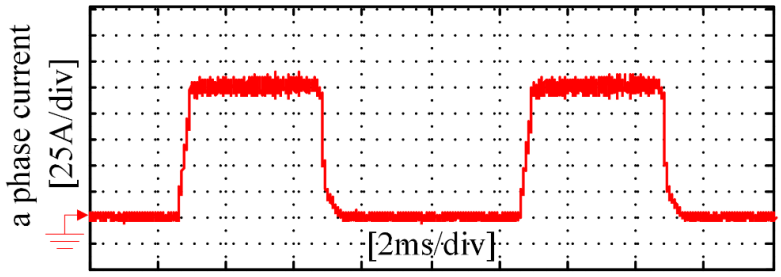

(b) Current Prediction at 10 kHz
Fig. 10. Experimental Current Waveforms at 1500 rpm

The current prediction algorithm demonstrates superior current-tracking performance, reducing current ripple by more than 50% compared to the chopping algorithm. This ensures that the actual current closely aligns with the reference value. Even under conditions where the rotor speed is doubled, the algorithm continues to exhibit stable and precise performance.

These findings highlight the algorithm's robustness and effectiveness in achieving accurate current control and mitigating oscillations. The experimental validation underscores the practical advantages of the proposed algorithm, confirming its ability to enhance system stability and achieve reliable operation in low-inductance SRMs across varying operational conditions.

6. Conclusion

The proposed fixed-frequency current prediction algorithm effectively addresses the challenge of severe current oscillations in low-inductance switched reluctance motors (SRMs). By discretizing the voltage equation and incorporating real-time rotor position measurements, the algorithm predicts the required RMS voltage for the next control step with high accuracy. To enhance model adaptability and reduce dependency on finite element analysis or neural network fitting, a Fourier-based curve fitting method is employed. This approach captures the characteristics of the incremental inductance across the entire rotor range using a compact and computationally efficient representation, enabling practical deployment in embedded control systems.

A key innovation of this work lies in its focus on low-speed current control performance, a condition where current ripple and tracking delays are typically more pronounced. Additionally, the integration of a one-step delay compensation mechanism explicitly accounts for microcontroller computation and sampling delays, thus improving real-time control accuracy and dynamic response. Compared to traditional model predictive control (MPC) frameworks, the proposed method features a simplified control architecture based on linearized predictive modeling and explicit current reference computation, making it highly suitable for

implementation on low-cost embedded platforms.

Simulation and experimental results confirm the effectiveness of the proposed method, achieving a current ripple reduction to within 6%, while significantly improving the overall stability and responsiveness of the SRM system. These findings highlight the method's potential as a robust, efficient, and scalable solution for current control in low-inductance SRMs. Future work will focus on further optimizing the algorithm for real-time applications across wider operating ranges and integrating it with advanced motor drive systems to enhance overall energy efficiency and control performance.

Acknowledgement

This work is supported by:

1) Heilongjiang Province key research and development plan guidance project "Soybean breeding intelligent sowing key technology Research and Agricultural implements development and Demonstration (GZ20220076);

2) Basic Research Support Program for Outstanding Young Teachers in Heilongjiang Provincial Universities (YQJH2023054).

REFERENCES

[1] *A. Chithrabhanu, & K. Vasudevan*, "A Novel Four Level Shared Switch Converter With Buck–Boost Energy Recovery Stage for Switched Reluctance Motor Drive", IEEE Journal of Emerging and Selected Topics in Industrial Electronics, **vol. 6**, no. 1, 2025, pp. 135-145. https://doi.org/10.1109/JESTIE.2024.3484214

[2] *X. Zhang, Q. Yang, M. Ma, Z. Lin, & S. Yang*, "A Switched Reluctance Motor Torque Ripple Reduction Strategy with Deadbeat Current Control and Active Thermal Management", IEEE Transactions on Vehicular Technology, **vol. 69**, no. 1, 2020, pp. 317-327. https://doi.org/10.1109/TVT.2019.2955218

[3] *A. Walz-Lange, & G. Schullerus*, "Sensorless Control of a Switched Reluctance Machine Based on Switching Frequency Evaluation", IEEE Transactions on Industry Applications, **vol. 58**, no. 4, 2022, pp. 4768-4777. https://doi.org/10.1109/TIA.2022.3173595

[4] *S. Dhale, B. Nahid-Mobarakeh, & A. Emadi*, "A Review of Fixed Switching Frequency Current Control Techniques for Switched Reluctance Machines", IEEE Access, **vol. 9**, 2021, pp. 39375-39391. https://doi.org/10.1109/ACCESS.2021.3064660

[5] *P. Tirapatsakorn, & F. Kucuk*, "Self-Initial Position Alignment of Incremental Encoder for Switched Reluctance Motor", 2023 4th International Conference on Advanced Electrical and Energy Systems (AEES), Shanghai, China, 2023, pp. 276-280. https://doi.org/10.1109/AEES59800.2023.10468697

[6] *J. Cai, X. Dou, A. D. Cheok, W. Ding, Y. Yan, & X. Zhang*, "Model Predictive Control Strategies in Switched Reluctance Motor Drives—An Overview", IEEE Transactions on Power Electronics, **vol. 40**, no. 1, 2025, pp. 1669-1685. https://doi.org/10.1109/TPEL.2024.3454819

[7] *J. Long, M. Yang, Y. Chen, D. Xu, & F. Blaabjerg*, "A Novel Voltage Injection Based Offline Parameters Identification for Current Controller Auto Tuning in SPMSM Drives", Energies, **vol. 13**, no. 11, 2020, pp. 3010. https://doi.org/10.3390/en13113010

[8] *J.I. Rocha, T.G. Amaral, D. Foito, A.J. Pires, & V.F. Pires*, "Fault Diagnosis Scheme Based on

the Stockwell Transform for a Multilevel Converter of a Switched Reluctance Motor Drive", 2024 13th International Conference on Renewable Energy Research and Applications (ICRERA), Nagasaki, Japan, 2024, pp. 1111-1116, https://doi.org/10.1109/ICRERA62673.2024.10815434

[9] *K. KAWARAZAKI, & N. HOSHI*, "Expansion of Switched Reluctance Motor Driving Range by Flux-weakening Control under Current Vector Control", 2024 13th International Conference on Renewable Energy Research and Applications (ICRERA), Nagasaki, Japan, 2024, pp. 1336-1341. https://doi.org/10.1109/ICRERA62673.2024.10815351

[10] *G. Demidova, A. Bogdanov, A. Iaremenko, Z. Xirong, H. Chen, & A. Anuchin*, "Neural Network Approaches for Magnetization Surface Prediction in Switched Reluctance Motors: Classical, Radial Basis Function, and Physics-Informed Models", 2024 IEEE 3rd International Conference on Problems of Informatics, Electronics and Radio Engineering (PIERE), Novosibirsk, Russian Federation, 2024, pp. 1270-1275. https://doi.org/10.1109/PIERE62470.2024.10804908

[11] *Z. Lin, D.S. Reay, B.W. Williams, & X. He*, "Torque Ripple Reduction in Switched Reluctance Motor Drives Using B-Spline Neural Networks", IEEE Transactions on Industry Applications, **vol. 42**, no. 6, 2006, pp. 1445-1453. https://doi.org/10.1109/TIA.2006.882671

[12] *J. Oloo, & L. Szamel*, "Rotor Position Sensing in Switched Reluctance Motors Using Magnetostrictive Amorphous Wire", 2024 IEEE 7th International Conference and Workshop Óbuda on Electrical and Power Engineering (CANDO-EPE), Budapest, Hungary, 2024, pp. 1-6. https://doi.org/10.1109/CANDO-EPE65072.2024.10772974

[13] *M. Karthika, & M. Balaji*, "Design and Performance Evaluation of 12/8 Hybrid Excitation of Switched Reluctance Motor for Electric Three-Wheeler", 2023 3rd International Conference on Innovative Mechanisms for Industry Applications (ICIMIA), Bengaluru, India, 2023, pp. 1421-1427. https://doi.org/10.1109/ICIMIA60377.2023.10426569

[14] *R. Mikail, I. Husain, Y. Sozer, M.S. Islam, & T. Sebastian*, "A Fixed Switching Frequency Predictive Current Control Method for Switched Reluctance Machines", IEEE Transactions on Industry Applications, **vol. 50**, no. 6, 2014, pp. 3717-3726. https://doi.org/10.1109/TIA.2014.2322144

[15] *J. Long, M. Yang, Y. Chen, K. Liu, & D. Xu*, "Current-Controller-Free Self-Commissioning Scheme for Deadbeat Predictive Control in Parametric Uncertain SPMSM", IEEE Access, **vol. 9**, 2020, pp. 289-302. https://doi.org/10.1109/ACCESS.2020.3043751